Rapid Communications

Ultrafast carrier dynamics in a GaN/$Al_{0.18}Ga_{0.82}N$ superlattice

Felix Mahler,[1] Jens W. Tomm,[1] Klaus Reimann,[1] Michael Woerner,[1] Thomas Elsaesser,[1] Christos Flytzanis,[2] Veit Hoffmann,[3] and Markus Weyers[3]

[1]*Max-Born-Institut für Nichtlineare Optik und Kurzzeitspektroskopie, 12489 Berlin, Germany*

[2]*Laboratoire Pierre Aigrain, École Normale Supérieure, 75231 Paris, France*

[3]*Ferdinand-Braun-Institut, Leibniz-Institut für Höchstfrequenztechnik, 12489 Berlin, Germany*

(Received 27 February 2018; revised manuscript received 13 April 2018; published 23 April 2018)

Relaxation processes of photoexcited carriers in a GaN/$Al_{0.18}Ga_{0.82}N$ superlattice are studied in femtosecond spectrally resolved reflectivity measurements at ambient temperature. The transient reflectivity reveals electron trapping into defect states close to the conduction-band minimum with a 150–200 fs time constant, followed by few-picosecond carrier cooling. A second slower trapping process into a different manifold of defect states is observed on a time scale of approximately 10 ps. Our results establish the prominent role of structural defects and disorder for ultrafast carrier dynamics in nitride semiconductor structures.

DOI: 10.1103/PhysRevB.97.161303

Nonequilibrium carrier dynamics in semiconductors occur on femto- to picosecond time scales and involve both carrier-carrier and carrier-phonon interactions [1]. Optical experiments in the ultrafast time domain together with theory and simulation have generated a quantitative picture of the relevant processes in III-V semiconductors. For carrier densities above some 10^{16} cm^{-3}, the initial nonequilibrium distributions of photoexcited electrons and holes thermalize into quasiequilibrium distributions at elevated temperature on a time scale of 100 fs. The resulting hot quasi-Fermi distributions cool down to lattice temperature by phonon emission, followed by slower processes of recombination and/or trapping into localized states. The high structural quality of bulk and nanostructured semiconductors from the (Ga-In-As-P) material system with atomically sharp interfaces between layers and low defect concentrations has been a key prerequisite for developing this detailed picture of elementary excitations and their coupling.

Current gallium nitride (GaN) based semiconductors display a much higher concentration of structural imperfections and defects [2,3]. As a result, the valence and conduction band continua are complemented by a large variety of defect states, in which electrons or holes are localized and/or excitons are bound to. Such states play a key role for the optical and transport properties of nitrides, as is evident from, e.g., photoluminescence spectra and studies of stimulated emission [4]. In addition to band-to-band and free and bound exciton transitions, defect-related optical bands cover a broad energy range below the band gap. Ultrafast carrier dynamics in this complex manifold of electronic states includes transitions between continuum and localized states opening additional scattering and relaxation channels.

Carrier dynamics in GaN semiconductors have been studied by time-resolved photoluminescence, which gives insight into recombination and—to a limited extent—trapping kinetics, and by femtosecond pump-probe techniques mapping transient absorption or reflection [5–9]. The latter reveal electron and hole redistribution on a time scale between several hundreds of femtoseconds and tens of picoseconds. They have mostly been interpreted in analogy to the carrier dynamics in (Ga-In-As-P) semiconductors. However, the interplay of continuum and localized states in carrier relaxation is far from being understood, in particular in low-dimensional quantum wells and superlattices, which play a central role in GaN-based optoelectronics.

In this Rapid Communication, we present a femtosecond pump-probe study of nonequilibrium carrier dynamics in an *n*-doped GaN/$Al_{0.18}Ga_{0.82}N$ superlattice (SL) with a doping level and structural parameters close to those of device structures. The interfaces between the layers introduce additional defects, which are characteristic for a broad range of GaN based quantum well, wire and dot structures. We directly measure carrier trapping times of a few hundred femtoseconds into defects close to the band extrema, followed by carrier cooling and a slower picosecond transfer of carriers into localized states.

The SL was grown by metal-organic chemical vapor deposition on a GaN buffer layer on a (0001) *c*-plane sapphire substrate. It consists of 60 periods of 3 nm GaN and 2 nm $Al_{0.18}Ga_{0.82}N$. The $Al_{0.18}Ga_{0.82}N$ barrier layers are *n*-doped with Si atoms of a concentration of 3×10^{18} cm^{-3}. To suppress chemical degradation, the sample was covered with a SiN $\lambda/4$ layer for a wavelength $\lambda = 350$ nm (photon energy 3.54 eV) [10]. Figure 1(a) shows the stationary reflectivity spectrum of the SL at room temperature (angle of incidence 8°), displaying a dispersive modulation in the range of the fundamental band gap of the SL.

The photoluminescence (PL) spectrum recorded in the same reflection geometry with continuous-wave excitation at 3.8 eV is shown in Fig. 1(a). Its main band with a maximum at 3.53 eV originates from interband transitions in the SL. The two shoulders at lower energies of 3.45 and 3.37 eV represent PL from the GaN buffer layer, generated by excitation light transmitted through the SL and by SL luminescence reabsorbed in the buffer layer (for details of this excitation mechanism see [11]).

The time-resolved pump-probe experiments were performed with an Yb-based laser system (Monaco; Coherent)

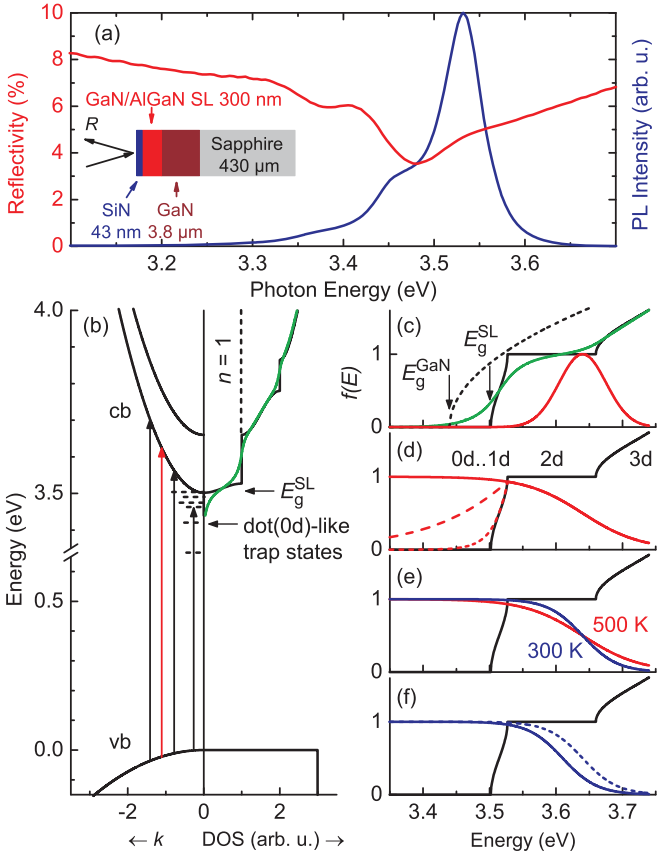

FIG. 1. (a) Stationary reflectivity spectrum (red line) and photoluminescence spectrum (excitation at 3.8 eV, blue line) of the SL sample with a SiN $\lambda/4$ top layer. The inset shows a schematic of the sample. (b) Band structure (left, cb: conduction band; vb: valence band) and the density of states (DOS, right) of the SL. The green line includes the contribution of trap states to the DOS. (c)–(f) Transient electron distributions at different stages of carrier relaxation (see text).

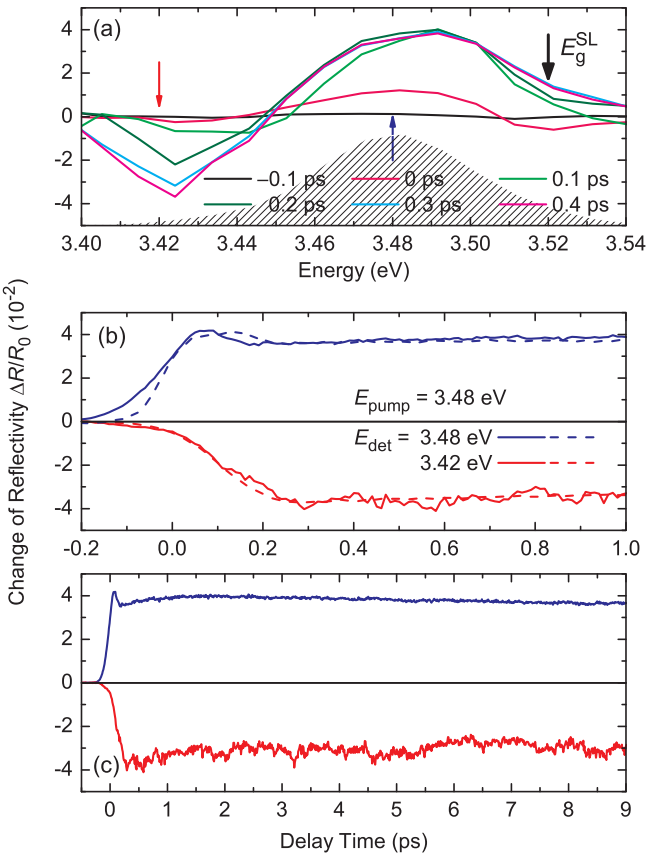

FIG. 2. (a) Transient reflectivity spectra of the SL sample for different pump-probe delays. The pump-induced reflectivity changes of the probe pulse are plotted as a function of photon energy. The arrows show the photon energies for the curves in (b) and (c) and the position of the SL gap, and the hatched area the pump spectrum. (b), (c) Time-resolved reflectivity changes at the photon energies indicated for pump-pulse energies of 6 nJ (solid lines) and 0.6 nJ (dashed lines). The 0.6 nJ curves are normalized to the corresponding 6 nJ curves.

pumping a noncollinear optical parametric amplifier (OPA) (Opera-F; Light Conversion). For the measurements, we generate the second harmonic of the signal pulses from the OPA. This second harmonic is tunable from 325 to 450 nm (3.8 to 2.8 eV) with average powers of up to 0.5 W at a repetition rate of 1 MHz. The pulse lengths as determined by a two-photon autocorrelator are below 50 fs at all wavelengths used. The linearly polarized pump and probe pulses are replicas of the OPA output with a pump-to-probe intensity ratio of 10.

Since the GaN layer below the SL absorbs at the transition energies of the SL, the pump-probe measurements are performed in a reflection geometry [Fig. 1(a)]. While the pump beam is incident normal to the surface, the direction of the probe beam is tilted by 30° from the normal for spatial separation of the two beams. The energy of the pump pulses is either 6 or 0.6 nJ on an area of $(25\ \mu\text{m})^2$, yielding a maximum carrier density per GaN well of 2.8×10^{13} cm^{-2} (2.8×10^{12} cm^{-2}) under the assumption that the pulse energy is absorbed completely in the SL. The pump beam is blocked periodically with a mechanical chopper. After interaction with the sample, the probe beam is spectrally dispersed in a 1/4 m grating monochromator with a spectral resolution of 2 nm (20 meV), and measured with a photodiode. The output from the photodiode is sent to a high-speed analog-digital converter that determines the required pump-induced reflectivity change $\Delta R/R_0 = (R - R_0)/R_0$ (R, R_0: sample reflectivity with and without excitation).

Pump-probe measurements in a spectral range close to the SL band gap at 3.52 eV were performed with pulses centered at 3.48 eV [for the spectrum see Fig. 2(a)]. The transient reflectivity spectra presented in Fig. 2(a) exhibit a negative and a positive reflectivity change $\Delta R/R_0$ of the probe pulse at low and high photon energies, respectively. Time-resolved reflectivity transients at fixed photon energies are shown in Figs. 2(b) and 2(c). It is important to note that the negative reflectivity change at 3.42 eV displays a delayed rise compared to the transients measured at higher photon energies, which show an onset within the time resolution of the experiment. Concomitantly, the negative component of the transient spectrum in Fig. 2(a) increases with a delay of 150–200 fs relative to the positive reflectivity change. On a longer time scale up to 10 ps, only gradual changes of the reflectivity signals are observed, which decay on a time scale of several hundreds of picoseconds.

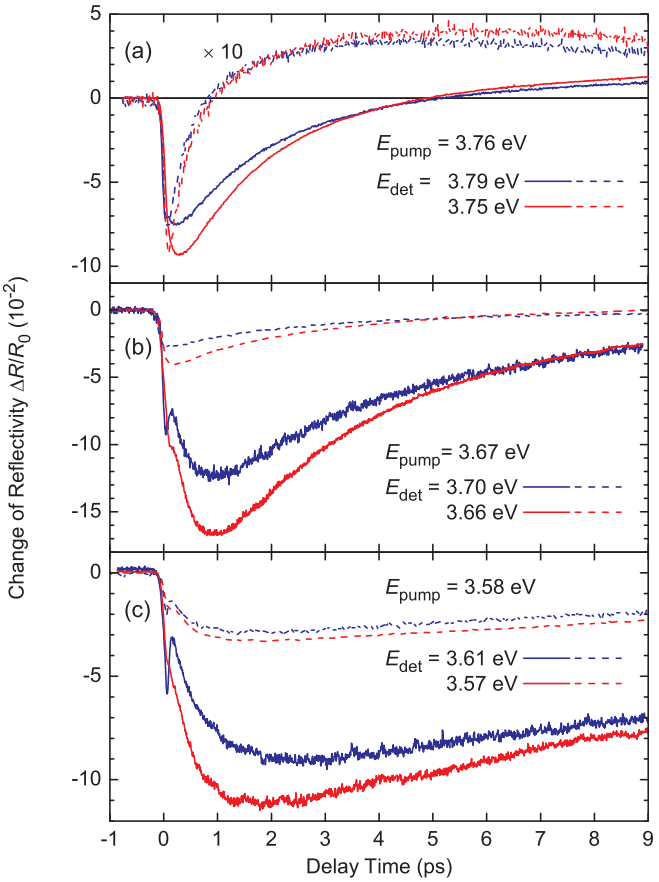

FIG. 3. Time-resolved reflectivity changes of the SL sample recorded with photon energies for pumping and detection as indicated. The solid lines show the data for 6 nJ pump-pulse energy, and the dashed lines for 0.6 nJ. In (a), the 0.6 nJ curve is shown multiplied by 10.

An analysis of our interaction geometry shows that the reflectivity changes originate mainly from changes of the real part of the refractive index of the SL [12], but with a change of the sign of the signal caused by the SiN layer on top of the SL. A pump-induced increase of the refractive index $\Delta n > 0$ of the SL without the SiN layer would lead to an increase of the reflectivity, i.e., a positive $\Delta R/R_0$, whereas in the present sample with the SiN layer on top a $\Delta n > 0$ leads to a decrease of the reflectivity and, thus, to a negative $\Delta R/R_0$. To summarize, the data in Fig. 2 exhibit a $\Delta n < 0$ with an instantaneous rise at high photon energies and a $\Delta n > 0$ with a delayed rise at low photon energies. This behavior is independent of the excitation density, as seen by the agreement between the data obtained with pump-pulse energies of 6 nJ (solid lines) and 0.6 nJ (dashed lines).

Figure 3 shows time-resolved transients at photon energies above the SL band gap. At high photon energies [Fig. 3(a)], the negative $\Delta R/R_0$ displays a fast rise, followed by a first decay and a slower evolution toward a positive $\Delta R/R_0$ at late delay times. The time for the first decay depends on the pump-pulse energy; it is about 2 ps for 6 nJ and 0.5 ps for 0.6 nJ. In contrast, the transients at lower photon energies show a biphasic rise with a first quasi-instantaneous component followed by a slower buildup within 2 ps. Their decay becomes slower with decreasing photon energy and covers a time range up to about 10 ps where a residual $\Delta R/R_0 < 0$ is reached.

We first explain the basic mechanism inducing the observed reflectivity changes. The sub-50-fs pump pulses excite electron-hole pairs in the SL and—to a much lesser extent—in the GaN buffer layer underneath the SL. Carriers excited in the SL are delocalized over many GaN layers because of the wave-function overlap along the SL stacking axis. The reflectivity changes measured by the probe pulses mainly arise from the interface between the SiN layer and the SL where the largest jump in refractive index occurs. At an excitation density of 10^{13} cm^{-2}, corresponding to a three-dimensional density of 3.3×10^{19} cm^{-3} per SL period, one gets a strong absorption decrease by Pauli blocking of interband transitions, i.e., band filling [13–15]. In parallel, the band gap of the excited sample is renormalized, resulting in a shift to smaller transition energies [16–21]. For an excitation density of 10^{19} cm^{-3}, one estimates a band-gap reduction by some 20 meV [22]. The strong changes of interband absorption are connected with changes of the refractive index, which are mapped in a spectrally and temporally resolved way in our femtosecond experiments.

The transient reflectivity data in Fig. 2 display strong changes of the refractive index Δn below the renormalized band gap of the SL at $E_g^{SL} \approx 3.5$ eV. Band filling in the SL minibands results in a $\Delta n < 0$ below the band gap [23], accounting for the positive reflectivity change $\Delta R/R_0$ observed between 3.45 and 3.5 eV [Fig. 2(a)]. This signal is mainly due to electron-hole pairs in states directly excited by the pump pulse and, thus, shows a quasi-instantaneous rise [Fig. 2(b)]. Below 3.45 eV, $\Delta R/R_0$ becomes negative, corresponding to $\Delta n > 0$. This signal is caused by the population of initially empty defect or trap states below the SL band gap, which display a nonzero transition dipole with valence-band states and, thus, contribute to the nonlinear changes of absorption and index of refraction. It is important to note that the reflectivity changes due to such defect states exhibit a delayed rise with a time constant of 150–200 fs. This rise time reflects the trapping kinetics of electrons from the SL miniband into the traps, a process temporally resolved here. The transients measured at early delay times at photon energies well above E_g^{SL} (Fig. 3) exhibit a negative $\Delta R/R_0$, in agreement with the positive index change Δn expected well above the band gap [23].

We now discuss the carrier relaxation manifested in the temporal and spectral evolution of the reflectivity changes. Figure 1(b) shows a schematic of the valence (vb) and conduction (cb) structures of the SL, plus a tail of trap states below the cb minimum, and the corresponding density of states (DOS). Optical excitation of electron-hole pairs to the SL miniband states above E_g^{SL} creates a nonequilibrium electron distribution $f(E)$ schematically shown in Fig. 1(c). Intraband carrier-carrier and carrier-LO phonon scattering establish hot quasiequilibrium distributions of electrons and holes in the minibands within our sub-100-fs time resolution [Fig. 1(d)]. At this initial stage, the LO phonon emission rate is very high because of the strong polar-optical coupling of GaN and leads to a rapid carrier cooling to temperatures between 300 and 500 K and to pronounced excess populations of LO phonon states.

After this initial intraminiband relaxation, electrons are transferred into the trap states close to the SL band edge,

resulting in an increase of $f(E)$ in this range [Fig. 1(d)]. The relevant time scale extends over hundreds of femtoseconds, as is evident from the data in Fig. 2. In parallel, the hot carrier distributions cool further down over a period of 1–2 ps, resulting in the decay of $\Delta R/R_0$ at photon energies probing states above the quasi-Fermi level E_F [Fig. 3(a)] and the picosecond rise of $\Delta R/R_0$ around E_F [Figs. 3(b) and 3(c)]. The picosecond kinetics are in line with previous studies of carrier cooling in nitride semiconductors at 300 K [6–9].

Carrier cooling is followed by slow kinetics extending to a delay time of approximately 10 ps. At the highest photon energies [Fig. 3(a)], the reflectivity changes $\Delta R/R_0$ become positive, while at the lower photon energies of Figs. 3(b) and 3(c) the amplitude of the negative $\Delta R/R_0$ becomes smaller. This behavior is caused by an overall population decrease in the SL minibands, moving the quasi-Fermi energy E_F and, correspondingly, the high-energy tail of the electron distribution closer to the SL band gap [Fig. 1(f)]. The loss in miniband population is due to slower trapping processes into a manifold of localized defect states, which are different from the trap states close to the conduction-band minimum and may cover a wide energy range in the GaN and AlGaN band gaps. Eventually, all reflectivity changes decay on a time scale of hundreds of picoseconds, similar to the photoluminescence decay (not shown).

For a theoretical analysis of the carrier relaxation and trapping scenario, one needs to consider different types of defects and the structural disorder in GaN/AlGaN nanostructures [4,24–26]. In the present SL with 2 nm, i.e., 8-monolayer-thick barriers containing 18% Al atoms, the random positions of Al atoms represent a prominent type of disorder. We solved the effective mass Schrödinger equation in real space in the envelope-function approximation [27] to find the energy eigenvalues and wave functions of this SL. We use one value of the potential for a lattice site with Al and one for a lattice site with Ga. The alloy is assumed to be ideal, i.e., every site has a probability of 18% to be occupied by Al, independent of the neighboring sites [28]. In contrast to the GaAs/AlGaAs system with a substantially smaller electron effective mass, the electron wave functions of the present GaN/AlGaN SL are not averaged over the alloy fluctuations in the barriers. As a result, an additional tail of eigenstates develops between the bulk GaN cb minimum and the cb edge of a SL without alloy fluctuations. The wave functions of electronic states in this tail display a dotlike character in the quantum well layers and a wirelike character in the barriers. As a result, these eigenfunctions are delocalized over two or more quantum wells along the growth direction and contribute to the interband absorption spectrum of the SL.

With the cb wave functions we calculated the corresponding electron–LO-phonon scattering rates [29] (because of the low Al concentration, only bulk GaN phonons are considered). The scattering rates essentially follow the density of final states in the cb of the alloy-disordered SL [green curves in Figs. 1(b) and 1(c)]. The calculated scattering times into unpopulated tail states are between 300 and 500 fs, in excellent agreement with the experimentally observed delayed rise at $E_{det} = 3.42$ eV [Fig. 2(b)]. For intraband cooling of electrons via LO phonon emission, one derives a rate of carrier temperature change $dT_C/dt \approx (T_L - T_C) \times 20\ \mathrm{ps}^{-1}$ with the LO phonon population at the lattice temperature T_L. The experimental cooling rates as seen in the delayed rise of the transients in Fig. 3(a) are substantially lower, which is caused by hot phonons [6,30]. This interpretation is supported by the faster rise for lower excitation densities where the density of generated phonons is lower.

In addition to the tail states originating from alloy disorder, there is a large variety of other defects in GaN/AlGaN structures. The total density of such defects is higher than both the doping concentration of the SL and the excitation density in the time-resolved experiments, so that a major fraction of such defect states is unpopulated. We assign the slow relaxation kinetics occurring on a 10 ps time scale (Fig. 3) to carrier trapping into such defects, leading to a reduction of the overall carrier density in the vb and cb continua and the observed reduction of the Fermi energy E_F.

In conclusion, our femtosecond pump-probe study of a GaN/AlGaN superlattice has revealed the prominent role of different types of defect states for ultrafast carrier relaxation. We distinguish a subpicosecond electron trapping into a tail of defect states close to the conduction-band minimum from slower trapping kinetics into other defects on a 10 ps time scale. Cooling of hot carriers occurs on a few-picosecond time scale and is slowed down by hot-phonon effects. The present relaxation scenario is relevant for a wide range of nanostructures made from nitride semiconductors.

[1] J. Shah, *Ultrafast Spectroscopy of Semiconductors and Semiconductor Nanostructures* (Springer, Berlin, 1999).

[2] R. A. Oliver, S. E. Bennett, T. Zhu, D. J. Beesley, M. J. Kappers, D. W. Saxey, A. Cerezo, and C. J. Humphreys, Microstructural origins of localization in InGaN quantum wells, J. Phys. D: Appl. Phys. **43**, 354003 (2010).

[3] A. Pinos, V. Liuolia, S. Marcinkevičius, J. Yang, R. Gaska, and M. S. Shur, Localization potentials in AlGaN epitaxial films studied by scanning near-field optical spectroscopy, J. Appl. Phys. **109**, 113516 (2011).

[4] M. A. Reshchikov and H. Morkoc, Luminescence properties of defects in GaN, J. Appl. Phys. **97**, 061301 (2005).

[5] C.-K. Sun, J.-C. Liang, X.-Y. Yu, S. Keller, U. K. Mishra, and S. P. DenBaars, Studies of carrier dynamics in unintentionally doped gallium nitride bandtail states, Appl. Phys. Lett. **78**, 2724 (2001).

[6] H. Ye, G. W. Wicks, and P. M. Fauchet, Hot electron relaxation time in GaN, Appl. Phys. Lett. **74**, 711 (1999).

[7] C. K. Choi, Y. H. Kwon, J. S. Krasinski, G. H. Park, G. Setlur, and J. J. Song, Ultrafast carrier dynamics in a highly excited GaN epilayer, Phys. Rev. B **63**, 115315 (2001).

[8] Y.-C. Huang, G.-W. Chern, K.-H. Lin, J.-C. Liang, C.-C. Hsu, S. Keller, and S. P. DenBaars, Femtosecond dynamics of exciton bleaching in bulk GaN at room temperature, Appl. Phys. Lett. **81**, 85 (2002).

[9] U. Özgür and H. O. Everitt, Ultrafast carrier relaxation in GaN, $In_{0.05}Ga_{0.95}N$, and an $In_{0.07}Ga_{0.93}N/In_{0.12}Ga_{0.88}N$ multiple quantum well, Phys. Rev. B **67**, 155308 (2003).

[10] C. Netzel, J. Jeschke, A. Knauer, and M. Weyers, Avoidance of instable photoluminescence intensity from AlGaN bulk layers, Phys. Status Solidi B **254**, 1600672 (2017).

[11] A. Maaßdorf, S. Gramlich, E. Richter, F. Brunner, M. Weyers, G. Tränkle, J. W. Tomm, Y. I. Mazur, D. Nickel, V. Malyarchuk, T. Günther, C. Lienau, A. Bärwolff, and T. Elsaesser, Minority-carrier kinetics in heavily doped GaAs:C studied by transient photoluminescence, J. Appl. Phys. **91**, 5072 (2002).

[12] The main contribution to the reflectivity signal is due to the wells near the SiN top layer. Contributions of the SL/GaN interface to the reflectivity change are expected to be negligible because of the small refractive index difference between SL and GaN and the attenuation of the beam reflected from this interface propagating twice through the SL. Absorption in the GaN buffer layer suppresses a contribution from its rear interface to the sapphire substrate.

[13] E. Burstein, Anomalous optical absorption limit in InSb, Phys. Rev. **93**, 632 (1954).

[14] T. S. Moss, The interpretation of the properties of indium antimonide, Proc. Phys. Soc. B **67**, 775 (1954).

[15] M. Feneberg, S. Osterburg, K. Lange, C. Lidig, B. Garke, R. Goldhahn, E. Richter, C. Netzel, M. D. Neumann, N. Esser, S. Fritze, H. Witte, J. Bläsing, A. Dadgar, and A. Krost, Band gap renormalization and Burstein-Moss effect in silicon- and germanium-doped wurtzite GaN up to 10^{20} cm^{-3}, Phys. Rev. B **90**, 075203 (2014).

[16] K. F. Berggren and B. E. Sernelius, Band-gap narrowing in heavily doped many-valley semiconductors, Phys. Rev. B **24**, 1971 (1981).

[17] G. W. Fehrenbach, W. Schäfer, J. Treusch, and R. G. Ulbrich, Transient Optical Spectra of a Dense Exciton Gas in a Direct-Gap Semiconductor, Phys. Rev. Lett. **49**, 1281 (1982).

[18] P. Vashista and R. K. Kalia, Universal behavior of exchange-correlation energy in electron-hole liquid, Phys. Rev. B **25**, 6492 (1982).

[19] P. Hawrylak, Electron-hole liquids and band-gap renormalization in short-period semiconductor superlattices, Phys. Rev. B **39**, 6264 (1989).

[20] M. Rinker, H. Kalt, K. Reimann, Y.-C. Lu, and E. Bauser, Band-gap renormalization in direct-band-gap $Al_xGa_{1-x}As$, Phys. Rev. B **42**, 7274 (1990).

[21] P. von Allmen, Plasmaron excitation and band renormalization in a two-dimensional electron gas, Phys. Rev. B **46**, 13345 (1992).

[22] M. Bouzidi, Z. Benzarti, I. Halidou, S. Soltani, Z. Chine, and B. El Jani, Photoreflectance investigation of band gap renormalization and the Burstein-Moss effect in Si doped GaN grown by MOVPE, Mater. Sci. Semicond. Process. **42**, 273 (2015).

[23] Y. H. Lee, A. Chavez-Pirson, S. W. Koch, H. M. Gibbs, S. H. Park, J. Morhange, A. Jeffery, N. Peyghambarian, L. Banyai, A. C. Gossard, and W. Wiegmann, Room-Temperature Optical Nonlinearities in GaAs, Phys. Rev. Lett. **57**, 2446 (1986).

[24] H. Morkoç, Comprehensive characterization of hydride VPE grown GaN layers and templates, Mater. Sci. Eng. **33**, 135 (2001).

[25] V. Yu. Davydov, I. N. Goncharuk, A. N. Smirnov, A. E. Nikolaev, W. V. Lundin, A. S. Usikov, A. A. Klochikhin, J. Aderhold, J. Graul, O. Semchinova, and H. Harima, Composition dependence of optical phonon energies and Raman line broadening in hexagonal $Al_xGa_{1-x}N$ alloys, Phys. Rev. B **65**, 125203 (2002).

[26] H. Morkoç, *Handbook of Nitride Semiconductors and Devices* (Wiley-VCH, Weinheim, 2008), Vol. 1.

[27] G. Bastard, Superlattice band structure in the envelope-function approximation, Phys. Rev. B **24**, 5693 (1981).

[28] If this condition is not fulfilled (clustering), there will be regions with higher and regions with lower Al concentrations, resulting in even more pronounced tail states.

[29] B. K. Ridley, Electron-phonon interaction in 2D systems, in *Hot Carriers in Semiconductor Nanostructures*, edited by Jagdeep Shah (Academic, Boston, 1992), pp. 17–51.

[30] P. Lugli, P. Bordone, L. Reggiani, M. Rieger, P. Kocevar, and S. M. Goodnick, Monte Carlo studies of nonequilibrium phonon effects in polar semiconductors and quantum wells. I. Laser photoexcitation, Phys. Rev. B **39**, 7852 (1989).